AIAA JOURNAL
Vol. 41, No. 2, February 2003

Decelerating Boundary Layer: A New Scaling and Mixing Length Model

A. Bernard,* J. M. Foucaut,† P. Dupont,† and M. Stanislas‡
Laboratoire de Mécanique de Lille, 59655 Villeneuve d'Ascq, France

A model experiment has been designed in the frame of a coordinated European project called AEROMEMS. This model is a two-dimensional bump in a boundary-layer wind tunnel, which mimics the adverse pressure gradient on the suction side of an airfoil at the verge of separation. The flow is characterized mainly by hot-wire anemometry. The integral parameters and the mean velocity profiles are compared to existing models and to Navier–Stokes computations. A new scaling and a new mixing length model are proposed and validated on the Ludwig and Tillman data also.

Nomenclature

C_f	=	skin-friction coefficient, $\tau_p/\frac{1}{2}\rho U_e^2$
C_p	=	pressure coefficient, $\Delta P/\frac{1}{2}\rho U_e^2$
$\mathrm{d}P/\mathrm{d}x$	=	pressure gradient, Pa/m
H	=	shape factor; see Eq. (5)
H_{12}	=	shape factor, δ^*/θ
H_{23}	=	shape factor, $1/H_{32}$
H_{32}	=	shape factor, δ^{**}/θ
h	=	height of the bump, m
l_m	=	mixing length
P	=	pressure, Pa
P^+	=	pressure gradient in wall units; see Eq. (6)
R_c	=	wall radius of curvature
Re_{δ^*}	=	Reynolds number based on the displacement thickness
Re_θ	=	Reynolds number based on the momentum thickness
s	=	curvilinear abscissa along the bump wall; origin at the top of the bump, m
U_e	=	external velocity, m/s
U_∞	=	freestream velocity, m/s
u, v	=	velocity components tangential and normal to the surface, m/s
u_p	=	scaling velocity of Durbin and Belcher[21]
u_s	=	scaling velocity of Perry and Shofield[12]
u'_s	=	modified scaling velocity
u_τ	=	friction velocity, m/s
u'	=	longitudinal turbulence intensity
u'_i	=	velocity fluctuations components, m/s
$\overline{u'_i u'_j}$	=	components of the Reynolds stress tensor, also $\overline{u'v'}$, etc.
u^+	=	mean velocity in wall units, u/u_τ
u'^+	=	longitudinal turbulence intensity in wall units, u'/U_τ
x, y, z	=	longitudinal, vertical, and transverse coordinates, m
y^+	=	normal coordinate in wall units, $y \cdot u_\tau/\nu$
α	=	curvature mixing length coefficient
β	=	nondimensional pressure gradient; see Eq. (6)
β'	=	nondimensional pressure gradient; see Eq. (6)
δ	=	boundary-layer thickness, m
δ^+	=	boundary-layer thickness in wall units, $\delta \cdot u_\tau/\nu$
δ^*	=	displacement thickness, m
δ^{**}	=	energy thickness, m
η	=	coordinate normal to the bump, m
η^+	=	coordinate normal to the bump in wall units, $\eta U_\tau/\nu$
θ	=	momentum thickness, m
κ	=	von Kármán constant
ν	=	fluid kinematic viscosity, m^2/s
ρ	=	fluid density, kg/m^3
τ	=	friction, $kg/m^2 \cdot s$
τ_w	=	wall friction, $kg/m^2 \cdot s$
χ	=	half-power mixing length coefficient

Received 1 February 2001; revision received 24 April 2002; accepted for publication 16 September 2002.

*Research Fellow; currently Research Engineer, LEA UMR 6609, Téléport 2, Boulevard Marie et Pierre Curie, 86962 Futuroscope Chasseneuil, France.
†Assistant Professor, UMR 8107, Bv. Paul Langevin, Cité Scientifique.
‡Professor, UMR 8107, Bv. Paul Langevin, Cité Scientifique.

I. Introduction

In the past 10 years, significant progress has been made in both numerical and experimental fluid dynamics. New tools are available that allow deeper insight in the physics of complex flows, including turbulence. Also, development of microelectromechanical systems is opening a new field of flow actuation at a small scale and at low energy cost.[1] The main advantage of such devices is that they could be integrated smoothly in the skin of the airfoil, acting only when needed. The control of the flow around an airfoil at high angle of attack is, of course, of strong interest. Such a flow is encountered in several flight phases (takeoff, landing, maneuver, etc.) and can lead to partial or large separation, with well-known consequences (vibration, drag increase, and loss of control). This is mainly because the boundary layer developing on the suction side is rapidly encountering a more or less strong adverse pressure gradient, which leads it more or less rapidly to separate. The turbulent boundary layer (TBL) submitted to an adverse pressure gradient (APG) is thus a subject of prime importance in aeronautics, and it has been studied quite extensively, both theoretically and experimentally, since the 1950s. The first reliable experiments mentioned are due to Ludwig and Tillman.[2] It is not the aim here to make a detailed review of the state of the art about this subject. Good reviews can be found by Coles and Hirt[3] and Spalart and Watmuff.[4] Only a few points relevant to the present contribution will be mentioned. In the present experiment, the TBL is submitted to both a varying pressure gradient and a varying wall curvature (going from convex to concave). Although many contributions could be cited, the effect of wall curvature can be summarized through the studies of So and Mellor,[5] Meroney and Bradshaw,[6] and Ramaprian and Shivaprasad.[7] On convex walls, even with mild curvature ($\delta/R_w \approx 0.01$), the effect is significant in the outer part of the BL. The strength of the wake is increased, but it deviates from the Coles[8] law. The shear stress and turbulence intensity decrease. The near-wall region is less affected, and the law of the wall holds. Along concave walls, for equivalent values of δ/R_w, unstable Görtler vortices appear, which lead to an increase of the turbulent shear stress and intensity and, in some cases, to the suppression of the law of the wall.

This law of the wall was shown to be fairly independent of the pressure gradient by Coles[8] in 1956, where he used the available

experimental results at that time to introduce his law of the wake. Coles suggested that δ should be proportional to $\delta^* Ue/u_\tau$. He also mentioned the idea of "equilibrium flow" as introduced by Clauser in 1954 for TBL submitted to adverse pressure gradients but keeping a universal velocity defect law. Coles showed that such "equilibrium TBL" should have a constant Π parameter. This idea of equilibrium TBL was developed by Townsend,[9] who gave it a theoretical basis linked to the equation for the turbulent kinetic energy. He introduced a difference between self-preserving flows and equilibrium layers. He notably showed that the law of the wall is linked to an equilibrium between strong production and dissipation of turbulent kinetic energy. He was also the first to infer the existence of a region varying with $\sqrt{y}$ in the mean velocity profile. An interesting contribution was made by Perry et al.[10] from the study of different nonequilibrium TBL. They introduced a decomposition of the wall region in three main regions and, from a similarity analysis, they could extend the Townsend theory[9] of the existence of a half-power-law region in the mean velocity profile above the law of the wall region, with a small blending region in between. Soon after, Perry,[11] by studying TBLs in decreasing APGs, extended the regional similarity hypothesis of Perry et al.[10] and showed evidence of regions of linear and $\frac{3}{2}$ power laws in the velocity profiles. This was explained by a stronger contribution of higher-order derivatives of the streamwise pressure distribution. Perry and Shofield[12] developed a velocity defect scaling based on a new velocity scale u_s determined by analogy with the Clauser plot but using the half-power law instead of the log law. The corresponding length scale was

$$B = 2.86\delta^*(U_e/u_s) \tag{1}$$

Samuel and Joubert[13] did a detailed study of a boundary layer developing in an increasingly adverse pressure gradient. (Thus, $\mathrm{d}P/\mathrm{d}x$ and $\mathrm{d}^2P/\mathrm{d}x^2$ were positive.) As will be seen, this situation corresponds to the beginning of the present APG region. The authors[13] obtained a fairly good verification of the law of the wall, all along the APG region of their flow. However, they showed that neither the half-power law of Perry et al.[10] nor the Townsend model[9] were able to represent the mean velocity profile above the log law. More recently, Dengel and Fernholtz[14] revisited the scaling proposed by Perry and Shofield.[12] Dengel and Fernholtz[14] showed that the mean velocity profiles were quite universal in this representation, but that they were best represented by an empirical seventh-order polynomial. The final contribution that should be mentioned here (without trying to be exhaustive on the subject of TBL submitted to an APG), is that of Skare and Krogstad[15] on an equilibrium TBL in strong APG. After redefining carefully the concept of equilibrium flow and its consequences for all mean flow properties, they did a careful experimental study, which showed that the gradient of the mixing length was increasing from $\kappa = 0.41$ near the wall to $\kappa = 0.78$ at the end of the log region. This did not influence the mean velocity profile, which followed closely the law of the wall with the usual coefficients. They also observed a strong production of turbulence in the outer part of the layer (around $y/\delta = 0.45$) accompanied by significant diffusion of turbulent kinetic energy toward the wall and by a strong dissipation also in the outer layer. As can be seen from this brief review, apart from the law of the wall, which seems to have a wide range of validity, unanimity is far from being reached, even for equilibrium APG TBL, on the universal representation of even the mean velocity profile.

II. Experimental Setup and Instrumentation

All of the measurements were performed in the Laboratoire de Mécanique de Lille boundary-layer wind tunnel. The boundary layer develops on the lower wall along a channel of constant cross section and 15 m long. It then enters a 5-m-long test section that has transparent walls. The tunnel section is 1×2 m^2. The maximum external velocity is 10 m/s, to allow Reynolds numbers Re_θ based on the momentum thickness between 7.5×10^3 and 2×10^4 to be obtained. This wind tunnel is computer controlled. The velocity is regulated better than 1% and the temperature better than 0.2°C during time periods of more than 8 h. This boundary layer has been characterized in detail by hot-wire anemometry in a previous study (Stanislas, M., Foucaut, J. M., Carlier, J., and Dupont, P., "Detailed Characterization of a High-Reynolds Number Boundary Layer, Part 1: Statistical Study," manuscript in preparation). The reference frame is chosen in the vertical plane of symmetry, attached to the lower wall. The x axis is along the wall and the flow, y is normal to the wall, and w is parallel to the wall and normal to the flow.

Table 1 Coordinates of the bump

x, m	Converging part y, m	s, m	x, m	Diverging part y, m	s, m
15.50	0.000	−1.549	17.20	0.325	0.202
15.60	0.002	−1.449	17.35	0.308	0.350
15.80	0.014	−1.249	17.40	0.300	0.400
16.00	0.044	−1.047	17.60	0.258	0.603
16.20	0.099	−0.840	17.63	0.251	0.640
16.40	0.178	−0.624	17.80	0.207	0.812
16.60	0.257	−0.408	17.90	0.181	0.918
16.80	0.310	−0.204	18.00	0.155	1.018
17.00	0.331	0.000	18.20	0.103	1.225
			18.24	0.093	1.267
			18.40	0.058	1.429
			18.58	0.031	1.611
			18.60	0.027	1.632
			18.80	0.006	1.833
			19.00	0.000	2.033

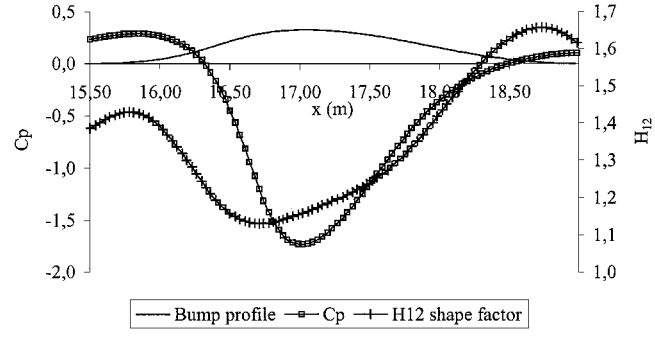

Fig. 1 Bump profile, computed pressure coefficient and BL shape factor.

The pressure gradient undergone by the boundary layer in the upstream 15 m of the channel is very small (−0.53 Pa/m at 10 m/s). To study a boundary layer in a significant adverse pressure gradient, the lower wall has been modified. A bump generates first a strong favorable pressure gradient and then an adverse pressure gradient. The shape of the bump has been computed at Dassault Aviation, using a two-dimensional Navier–Stokes solver with a k–ε turbulence model, to avoid separation in front of the bump and to generate an adverse pressure gradient representative of an airfoil at high angle of attack. This shape is presented in Fig. 1. Care was taken to bring the boundary layer on the verge of separation but to prevent it from separating, to avoid three-dimensional perturbations. Table 1 gives the coordinates of the bump in the reference frame of the wind tunnel. The last column is the curvilinear abscissa s along the bump with the origin taken at the point of maximum height. In Fig. 1 the computed pressure coefficient C_p and shape factor H as a function of x are also given. The shape factor reaches a maximum value of 1.66 at $x = 18.70$ m, which is just the end of the bump. This value is characteristic of a strongly destabilized BL, which is not very far from separation. The bump has the shape of a half-airfoil. It has a maximum height of 0.33 m above the floor of the wind tunnel and a length of 3.40 m. Its angle of incidence can be adjusted within ±3 deg to adjust the pressure gradient at best to the computations. A careful alignment of the model allows keeping the whole surface within ±2 mm from the profile defined by the Navier–Stokes computations.

To characterize the basic flow, mainly hot-wire anemometry was used. In the present study, only single wire probes were used. They were manufactured by AUSPEX with platinum plated tungsten wires 2.5 μm in diameter and 0.5 mm in length. These probes were approached at 0.2 mm from the wall. The probes were mounted on a traversing system, which was computer controlled. Calibration was

Table 2 Pressure distribution obtained from experiment and computation

x, m	s, m	C_p experiment	dP/dx experiment, Pa/m	dC_p/dx experiment	C_p computation	dP/dx computation, Pa/m	dC_p/dx computation
17.35	0.350	−1.322	78.4	0.705	−1.425	78.5	0.601
17.63	0.640	−0.805	84.1	0.893	−0.923	80.6	0.743
17.90	0.918	−0.382	57.3	0.700	−0.460	57.3	0.635
18.24	1.267	——	30.2[a]	0.425	−0.142	30.2	0.398
18.58	1.611	——	13.4[a]	0.200	−0.034	13.4	0.196

[a]Estimated.

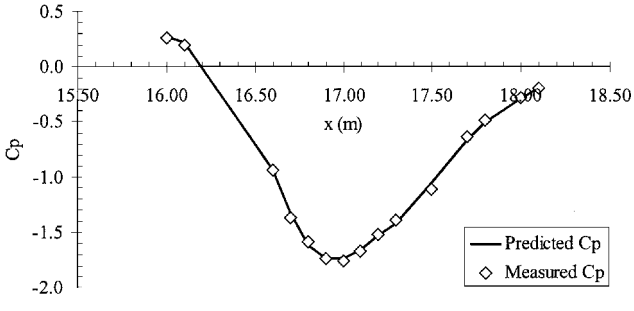

Fig. 2 Comparison between computed and measured pressure distribution.

performed at midheight of the wind tunnel, in a region where the velocity profile is uniform. The probes were connected to a four-channel AN-1003 AAlab hot-wire anemometer. The signal from the anemometer was low-pass filtered at 5.5 kHz and digitized by a personal computer equipped with an A/D converter board and a sample and hold circuit. The acquisition frequency was 11 kHz, and 1.1×10^6 samples were taken for each measurement point. Calibration and measurements were fully computer controlled, with temperature and velocity regulation. The temperature was the same for the calibration and the measurements. Five stations were chosen for the characterization of the flow without control. They are shown subsequently. The traversing system was adjusted normal to the wall at each station. The two-dimensional character of the flow was checked both by spanwise pressure measurements and by the wool tuffs technique. This technique was applied both on the bump and on the ceiling of the wind tunnel to check that no separation or important corner vortices were present.

III. Results

A. Global Characteristics

Detailed pressure measurements were performed to ensure the two dimensionality and to characterize the pressure distribution. This was done using a Furness FC014 micromanometer pressure transducer with a full range of 10-mm H_2O. The accuracy on these measurements was ±0.1 Pa. The pressure coefficient was computed based on the upstream outer velocity:

$$C_p = (P - P_a) \Big/ \tfrac{1}{2}\rho U_\infty^2 \tag{2}$$

Figure 2 gives the measured streamwise distribution of C_p, as compared to the predictions obtained by Dassault Aviation using the two-dimensional Navier–Stokes solver with a k–ε turbulence model.[16,17] The numerical values are gathered in Table 2. As can be seen, the agreement is quite good between the two results. This was obtained by adjusting carefully the angle of incidence of the bump.

Table 3 gives the global parameters deduced from the measured velocity profiles as a function of the abscissa x and the curvilinear coordinate s (origin at $x = 17$ m, which is the top of the bump) and Table 4 the same parameters but provided by the Navier–Stokes computations and using the modulus of the velocity to compare at best with the single hot-wire experimental results. For the experiments, the skin friction is deduced from a Clauser plot, supposing that the von Kármán constant is $\kappa = 0.41$. The local skin-friction coefficient is

$$C_f = \tau_p \Big/ \tfrac{1}{2}\rho U_e^2 \tag{3}$$

Table 3 Global parameters of the BL: experiments

	x, m				
Parameter	17.35	17.63	17.90	18.24	18.58
s, m	0.350	0.640	0.918	1.267	1.611
U_e, m/s	13.61	12.53	11.68	10.88	10.56
δ, m	0.115	0.188	0.249	0.364	0.455
δ^*, m	0.0066	0.0169	0.0329	0.0618	0.0782
θ, m	0.0053	0.0128	0.0224	0.0363	0.0462
δ^{**}, m	0.0099	0.0234	0.0396	0.0662	0.0784
H_{12}	1.24	1.319	1.471	1.703	1.693
H_{32}	1.858	1.820	1.772	1.715	1.697
H	1.18	1.05	0.95	0.87	0.85
C_f	0.0031	0.0017	0.0008	0.0003	0.0005
U_τ, m/s	0.535	0.365	0.240	0.140	0.165
Re_θ	4,887	10,501	17,131	26,112	32,384
Re_{δ^*}	5,988	14,117	25,618	44,825	55,052
δ^+	4,293	5,765	4,399	4,975	5,308
P^+	0.0064	0.0216	0.0518	0.1376	0.0373
β	1.51	8.89	27.27	79.35	32.07
β'	0.059	0.259	0.560	1.021	0.501

Table 4 Global parameters of the BL: computations

	x, m				
Parameter	17.35	17.63	17.9	18.24	18.58
s, m	0.350	0.640	0.918	1.267	1.611
U_e, m/s	14.75	13.45	12.26	11.26	10.67
δ, m	0.137	0.178	0.235	0.316	0.334
δ^*, m	0.0059	0.0128	0.0256	0.0479	0.0677
θ, m	0.0047	0.0098	0.0178	0.0284	0.0361
δ^{**}, m	0.0088	0.0179	0.0314	0.0480	0.0593
H_{12}	1.246	1.303	1.433	1.688	1.876
H_{32}	1.852	1.819	1.761	1.690	1.643
H	1.15	1.05	0.93	0.84	0.80
C_f	0.0069	0.0037	0.0015	0.0007	0.0009
U_τ, m/s	0.868	0.578	0.336	0.217	0.232
Re_θ	4,658	8,822	14,581	21,298	25,668
Re_{δ^*}	5,804	11,496	20,897	35,941	48,151
δ^+	7,928	6,859	5,264	4,571	5,166
P^+	0.0015	0.0052	0.0189	0.0369	0.0134
β	0.51	2.58	10.81	25.61	14.04
β'	0.030	0.111	0.296	0.494	0.305

and the friction velocity

$$u_\tau = \sqrt{\tau_p/\rho} \tag{4}$$

Here δ is the boundary-layer thickness, which was estimated but is surely the less accurate parameter in such a situation because the velocity profiles does not show a clear constant velocity region. From the integral lengths, δ^*, θ, and δ^{**}, different shape factors can be computed:

$$H_{12} = \delta^*/\theta, \qquad H_{32} = \delta^{**} \Big/ \theta (= 1/H_{23})$$

$$H = 0.5442 \cdot H_{23} \sqrt{H_{23}/(H_{23} - 0.5049)} \tag{5}$$

This modified shape factor was introduced by Truckenbrodt[18] and is mentioned by Schlichting[19] as a more reliable separation criterion. The range $0.723 < H < 0.761$ is characteristic of velocity profiles

prone to separate, and the value $H = 1$ is the limit between favorable and adverse pressure gradient.

As can be seen, in the experiments, the boundary-layerthickness increases very rapidly in the decelerating region. This is accompanied by a strong variation of the shape factor H_{12}, which stabilizes itself around 1.7 at $x = 18.24$ m. The H_{32} shape factor is less sensitive and shows only a small decrease. The H shape factor is decreasing rapidly toward separation values at the first three stations, but stabilizes itself above the critical value at the last two stations. The values obtained for H_{12}, H_{32}, and H in the present experiment are in fairly good agreement with the model given by Schlichting[19] (page 675, Fig. 22.6). As expected, the skin friction decreases continuously along the studied region (see C_f and u_τ). The two characteristic Reynolds numbers Re_θ and Re_{δ^*} do logically increase rapidly with x whereas the boundary-layerthickness, scaled in wall units, is kept nearly constant.

The computational results of Table 4 show a slight underestimation of the integral parameters and a significant overestimation of the skin friction, especially at the first station. The shape factors are in fairly good agreement, especially the H shape factor of Truckenbrodt.[18] Globally, the agreement is fairly good except at the first station. This will be confirmed by the velocity profiles.

In Fig. 3, the external velocity is plotted as a function of the curvilinear abscissa along the wall. Also plotted in Fig. 3 is a theoretical distribution obtained by writing the conservation of mass with a flow rate velocity of 9.4 m/s on the full height of the tunnel (1 m). For this estimation of U_e, the height of the bump was taken in the section of the top of the boundary layer for each station. The displacement thickness on the bump was added to this height. No account was taken of the displacement thickness on the upper wall because the boundary layer is not known there. The flow rate velocity used takes into account that the regulation velocity was fixed at 10 m/s with a pitot tube located 0.35 m behind the end of the bump and at 0.41 m from the upper wall. This regulation velocity is, thus, slightly larger than the flow rate velocity. As can be seen from Fig. 3, the theoretical values are in fair agreement with the experimental results. An inflexion point appears on the experimental data at $s = 0.5$ m, which corresponds to the middle of a nearly constant pressure gradient zone in Fig. 1.

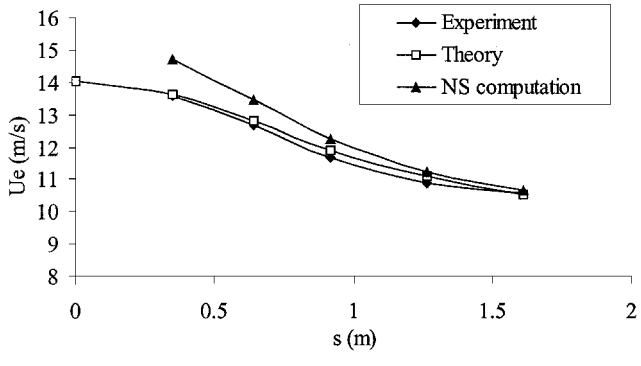

Fig. 3 External velocity along the diverging part of the bump: comparison between experiment, theory, and computation.

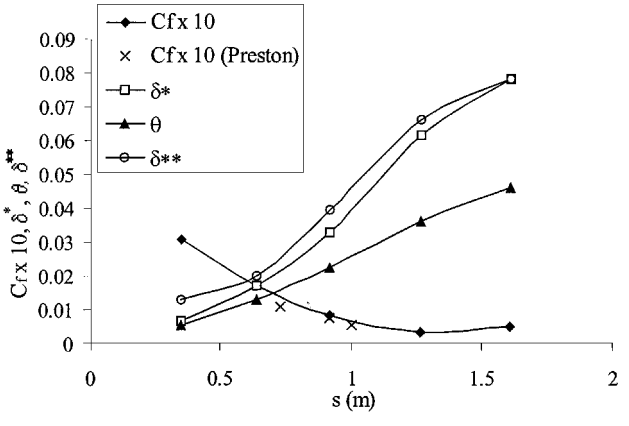

Fig. 4 Distribution of skin-friction coefficient, displacement, momentum, and energy thicknesses along the bump.

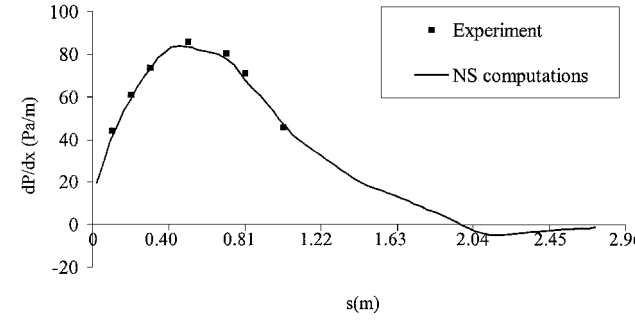

Fig. 5 Pressure gradient along the bump; comparison between experiment and computations.

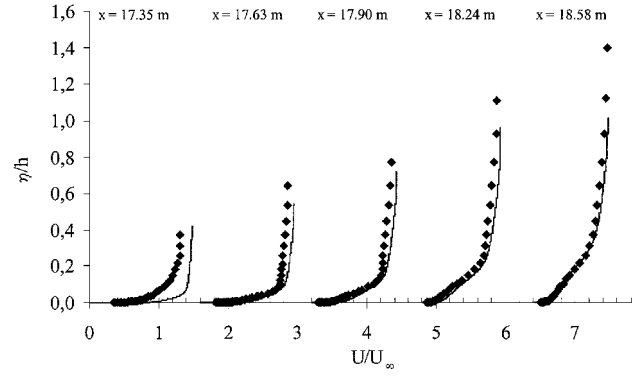

Fig. 6 Mean velocity profiles compared to Navier–Stokes computations at Dassault.

In Fig. 4, the friction coefficient, the displacement, momentum, and energy thickness from the experiment are plotted as a function of s. Validation measurements of C_f at three stations with Preston tubes are also shown in Fig. 4. All data show an inflexional behavior analogous to that of the external velocity. The inflexion point is farther downstream, around $s = 0.80$ m. This behavior is quite far from what is observed in an equilibrium flow (private communication, Elsberry, K., Loeffler, J., Zhou, M., and Wygnanski, I., "An Experimental Study of a Boundary Layer That Is Maintained on the Verge of Separation," 2000), where δ and θ grow linearly with s, whereas U_e follows a decreasing power law.

To conclude on the global characteristics, Table 3 gives a few parameters associated to the pressure gradient:

$$P^+ = \frac{1}{\rho}\frac{\mathrm{d}P}{\mathrm{d}x}\frac{\nu}{u_\tau^3}, \qquad \beta = \frac{1}{\rho}\frac{\mathrm{d}P}{\mathrm{d}x}\frac{\delta^*}{u_\tau^2}, \qquad \beta' = \frac{1}{\rho}\frac{\mathrm{d}P}{\mathrm{d}x}\frac{\delta^*}{Ue \cdot u_\tau} \tag{6}$$

The parameter P^+ is simply the pressure gradient scaled in wall units. The coefficient β was introduced by Clauser, based on the von Kármán integral equation, and is often used as an external scaling of the pressure gradient. The last parameter will be discussed further later. Nevertheless, it appears from Table 3 that all three parameters show a rapid increase with x with an extremum around $x = 18.24$ m and a sharp decrease after this station.

Figure 5 gives a comparison between the values of the pressure gradient deduced from the pressure measurements and from the Navier–Stokes two-dimensional computation with a k–ε model. The agreement is observed to be fairly good. The differences observed between Tables 3 and 4 for the parameters P^+, β, and β' are mainly due to the overprediction of the skin friction by the computation.

B. Mean Velocity Profiles

Figure 6 gives the mean velocity profiles obtained by hot-wire anemometry at the five stations along the wall. The ordinate η is

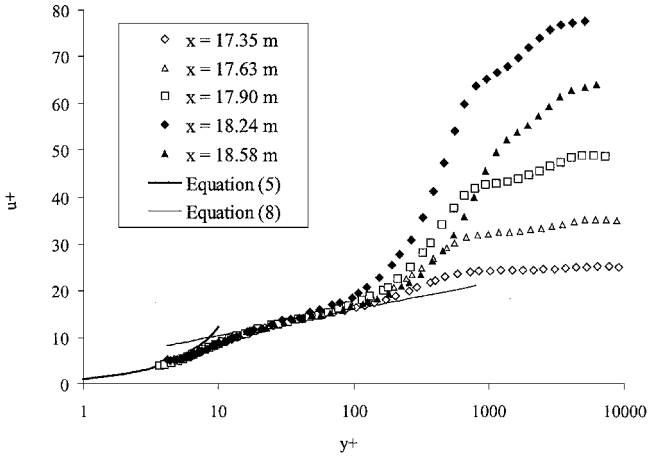

Fig. 7 Logarithmic plot of the mean velocity profiles in wall units at the five measurement stations.

normal to the wall at each station. It is normalized by the maximum height of the bump $h = 0.33$ m. The velocity is normalized by U_∞. These results are also compared to the predictions performed by Dassault, using the k–ε model. The experimental results clearly show the effect of the adverse pressure gradient. The momentum flux decreases very rapidly in the near-wall region, and a fairly linear region can be clearly detected at $x = 18.24$ and 18.58 m. The computational results overestimate the near-wall momentum at the first station, but the agreement is fairly good at the last four. This indicates that the model used overestimates the downstream influence of the favorable pressure gradient region located upstream of the top of the bump.

Figure 7 gives a logarithmic representation of the velocity profiles in wall variables. Also plotted in Fig. 7 is the modified velocity profile in the viscous sublayer, due to the pressure gradient:

$$u^+ = y^+\left(1 + \frac{P^+}{2}y^+\right), \qquad P^+ = \frac{1}{\rho}\frac{\mathrm{d}P}{\mathrm{d}x}\frac{\nu}{u_\tau^3} \tag{7}$$

and the classical log law

$$u^+ = 2.44\ln(y^+) + 4.7 \tag{8}$$

As observed by previous authors, a logarithmic region exists on all profiles, which is well represented by Eq. (8) and which is common to the five stations in this representation. Its extension decreases significantly when the adverse pressure gradient increases. The buffer layer exists in all cases and is well captured by the measurements, which stop at the limit of the viscous sublayer. The effect of the pressure gradient appears mainly in the wake region, which strongly develops with s and reduces the extend of the log region. This wake region is observed to split into two parts, separated by an abrupt change in the slope of the profile.

As was mentioned earlier, a region where u^+ behaves as $\sqrt{y^+}$ can be shown theoretically in the fully turbulent part of the inner region, with the hypothesis that the nondimensional pressure gradient P^+ is large compared to 1 (Ref. 9). In the present study, this region was sought. It can be detected just above the log region. Its extent is fairly limited and reduces from the first to the last station, where it nearly disappears. In fact, the hypothesis that $P^+ \gg 1$ is not necessary and, on the basis of the mixing length model, with $l_m = \kappa \cdot y$, the momentum equation can be integrated in this region to give the following velocity profile:

$$u^+ = (2/\kappa)\sqrt{1 + P^+y^+} - (2/\kappa)\,\mathrm{arcth}\left(1\Big/\sqrt{1 + P^+y^+}\right) + C \tag{9}$$

where C is an arbitrary constant and $\kappa = 0.41$ the von Kármán constant. This equation is in fact similar to the one proposed by Townsend.[9] The best fit of the model to the data was sought and is not shown here. C is not universal and takes the values given in Table 5 at the different stations. Compared to the simple log law, this model also allows the trend of the first part of the wake region to be predicted. This prediction is better (but not perfect) at $x = 17.35$ m than at $x = 18.24$ m, where it gives only the general upward trend of the velocity profile.

Table 5 Values of the constants in theoretical laws (9), (11), (14), (15), and (22)

x, m	s, m	C	E	u_s	u'_s	χ	D
17.35	0.350	15.5	15.2	12.3	0.132	1	11.5
17.63	0.640	11.63	11.6	14.1	0.128	1.26	11.5
17.90	0.918	8.5	/	16.7	0.119	1.5	11.6
18.24	1.267	5	/	18.2	0.108	1.9	11.5
18.58	1.611	9.5	9.5	15.5	0.085	1.5	11.6

In the model of Eq. (9), only the influence of the pressure gradient has been looked for. In fact, in the present case, the boundary layer is submitted to a variable adverse pressure gradient and also to a variable wall curvature changing from convex to concave with a fairly long flat surface in between. As discussed in the Introduction,[5–7] it can be expected that the mean velocity profile is affected by this curvature. Only the first and the last measurement stations are directly subject to wall curvature of opposite sign. The radius of curvature is $R_c = +1.27$ m at $x = 17.35$ m and $R_c = -1.74$ m at $x = 18.58$ m. Thus, following the literature, the wake region should be affected at the first station and the near-wall region at the last one. At $x = 18.58$ m, different from the study of So and Mellor,[5] the log region is still present (Fig. 7). Following Cousteix,[20] it is possible to introduce a modification of the mixing length model of the form

$$l_m = \kappa y[1 - \alpha(y/R_c)] \tag{10}$$

where R_c is the radius of curvature of the wall, which is positive when the wall is convex, and α should be of the order of 10.

With such a model, the velocity profile in the fully turbulent part of the inner region becomes

$$u^+ = -\frac{2}{\kappa}\,\mathrm{arcth}\left(\frac{1}{\sqrt{1 + P^+y^+}}\right) + \frac{2}{\kappa}\left(1 + \frac{P^+}{\alpha}Re_c^+\right)\cdot\mathrm{arcth}\left(\frac{\sqrt{1 + P^+y^+}}{\sqrt{1 + (P^+/\alpha)R_c^+}}\right) + E \tag{11}$$

with E an arbitrary constant.

The best fit of this model was also sought. The value of α was 25 at all relevant stations, and the values of E are given in Table 5. The prediction is significantly improved at $x = 17.35$ m. The profile is correctly represented up to the slope change of wake region. This model also brings an improvement, with $R_c = 1.7$ m, at $x = 17.64$ m, where the wall has just flattened. One can suspect that the streamlines are still curved at this station. At $x = 18.58$ m, the wall curvature seems to act in the wrong direction, indicating that phenomenon other than curvature should be more important there.

At this stage, the question arises as to whether the region above the log law should scale in wall variables or whether more appropriate characteristic parameters could be found. Attempts to fit classical wake functions such as Coles's[8] law of the wake were not successful. From Fig. 7, it appears that the region localized just above the log region, which spreads roughly between $y^+ = 100$ and 1000, is intermediate between the wall region and an external wake region. Such a region should scale neither in wall variables nor in external variables. This was more or less identified by Durbin and Belcher[21] in their proposal of local scaling velocity based on the pressure gradient:

$$u_p = \left(\frac{1}{\rho}\frac{\mathrm{d}P}{\mathrm{d}x}\frac{\nu}{u_\tau^3}\right)^{\frac{1}{3}} \tag{12}$$

The nondimensional variables are then

$$\hat{u} = u/u_p, \qquad \hat{y} = yu_p/\nu \tag{13}$$

An attempt was made to fit this model to the present experimental results, but this representation shows poor universality in this case.

Another proposal, which appears quite successful for that region, is that of Perry and Shofield,[12] which has been revisited by Dengel and Fernholtz.[14] The latter authors use a defect law representation with a scaling velocity u_s determined by fitting the following equation:

$$(u/U_e) = 0.47(u_s/U_e)^{\frac{3}{2}}(y/\delta^*)^{\frac{1}{2}} + 1 \cdot -(u_s/U_e) \qquad (14)$$

to the half-power-law part of the profile.

The values of u_s obtained from the slope coefficient of Eq. (14) are given in Table 5. In agreement with the findings of Dengel and Fernholtz (Ref. 14, Fig. 5), u_s is generally larger than U_e. This means that the scaling velocity inside the shear layer is larger than the maximum velocity of the flow at that station. This makes the physical interpretation of u_s difficult, and in the present case, the velocity profiles are not universal in this representation. Nevertheless, note that Dengel and Fernholtz do find universal profiles for boundary layers around the separation region, but with much larger values of the shape factor than in the present case ($2.2 < H_{12} < 4$). The wake region does not appear to scale on external variables. Thus, a second attempt was made to fit a wall law to the half-power region:

$$u/u'_s = (2/\kappa)(y \cdot u'_s/\nu)^{\frac{1}{2}} + F \qquad (15)$$

with $\kappa = 0.41$. The corresponding values of u'_s are given in Table 5. As can be seen, in this case, the values of u'_s are of the same order of magnitude as u_τ, but vary much slower with x. The scaling velocity can, thus, be interpreted as more representative of the friction in the inner wake region than u_τ. If the $\overline{u'v'}$ profile were available, it would be worthwhile to compare u'_s to $\sqrt{(\tau/\rho)}$ in this region. With this new velocity scale, the defect law of Perry and Shofield[12] becomes

$$(U_e - u)/u'_s = f(y/B) \qquad (16)$$

With $B = 2.86\delta^* U_e/u'_s$, the profiles at the last three stations (corresponding to the larger values of H) tend toward a common part in this inner wake region.

In fact, because the boundary layer under study is at an early stage toward separation, u_τ is still significantly different from zero and, thus, can be considered to be still representative of the inner region as a velocity scale. One can then question the choice of the length scale because this inner wake region is farther from the wall. By analogy to the initial idea of Coles[8] to estimate an external length scale from the displacement thickness δ^* as

$$\delta \approx \delta^*(U_e/u_\tau) \qquad (17)$$

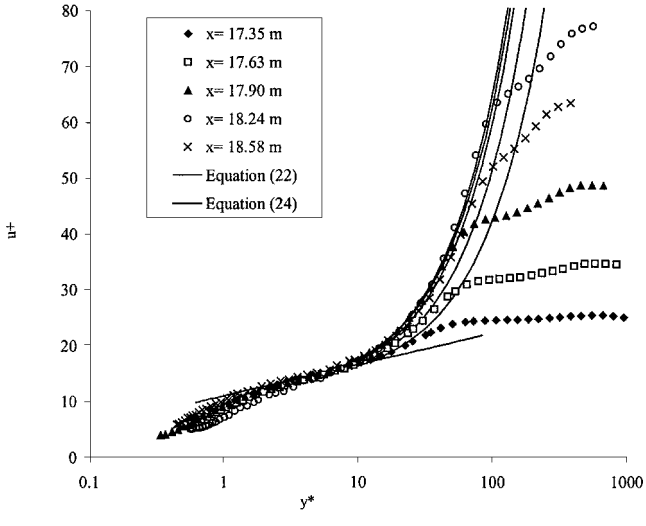

Fig. 8 Logarithmic plot of the mean velocity profiles in mixed units at the five measurement stations compared to Eqs. (22) and (24).

one can propose to define an inner scale as

$$l \approx \delta^*(u_\tau/U_e) \qquad (18)$$

With such a definition, it is possible to scale the wall distance in the following way:

$$y^* = (y/\delta^*)(U_e/u_\tau) \qquad (19)$$

Figure 8 gives u^+ as a function of y^* at the five measurement stations. The intermediate wake region appears to tend toward a universal profile as the adverse pressure gradient increases. This asymptotic profile, corresponding to $x = 18.24$ m, appears to be nearly linear. Taking into account the longitudinal momentum equation which is

$$\frac{\mathrm{d}}{\mathrm{d}y}\left(\mu_t \frac{\mathrm{d}u}{\mathrm{d}y}\right) = \frac{\mathrm{d}P}{\mathrm{d}x}, \qquad \mu_t = \rho \cdot l_m^2 \cdot \left|\frac{\mathrm{d}u}{\mathrm{d}y}\right| \qquad (20)$$

and neglecting the convection terms, one can propose the following mixing length law for that region:

$$l_m^* = \chi\sqrt{y^*} \qquad (21)$$

Such a mixing length leads to the following form of the mean velocity profile:

$$u^+ = (1/\chi)\Big[\sqrt{y^*(1+\beta' y^*)} + \left(1\Big/\sqrt{\beta'}\right)\ln\left|\beta'\sqrt{y^*} + \sqrt{1+\beta' y^*}\right|\Big] + D \qquad (22)$$

where D is an arbitrary constant and β' is the nondimensional pressure gradient in the following form:

$$\beta' = \frac{1}{\rho}\frac{\mathrm{d}P}{\mathrm{d}x}\frac{\delta^*}{U_e \cdot u_\tau} = \beta\frac{u_\tau}{U_e} \qquad (23)$$

In Fig. 8, together with the experimental results, the predictions with the model of Eq. (22), where χ and D were optimized for each station, are presented. The corresponding values of χ and D are given in Table 5. As can be seen, the velocity profiles in the intermediate region are fairly well represented by the model. This is particularly true for all but the first one ($x = 17.35$ m), which was shown earlier to be affected by curvature, a parameter which is not taken into account in Eq. (18). At the first two stations, departure is observed in the outer part of the inner wake region, which is in agreement with the literature concerning the effect of convex curvature. Figure 8 also shows that both the experiment and the model tend toward a nearly universal profile at the last three stations. This was also found with the u'_s scaling but mainly at the last two stations. Also plotted in Fig. 8, is the logarithmic Eq. (8), which, in this representation, is

$$u^+ = 2.44\ln y^* + \ln\left(U_e\delta^*\Big/\nu\right) \cdot (u_\tau/U_e)^2 + 4.7 \qquad (24)$$

The value of the constant, which is now a function of the Reynolds number, varies between 10 and 11 at the various stations. The curve represented in Fig. 8 corresponds to a constant value of 11. Table 5 shows that D is nearly constant and that χ is varying with the pressure gradient. To characterize this variation, the relation between χ and β' has been investigated. A least-square fit gives

$$\chi = 1 + 0.9\beta' \qquad (25)$$

with a correlation coefficient $R^2 = 0.98$.

Thus, it can be concluded from the present results that the mean velocity profile follows faithfully the law of the wall at all stations. As the flow progresses in the adverse pressure gradient, the log region reduces in extent, while an inner wake region develops above it. This inner wake region shows a linear velocity profile, corresponding to a half-power mixing length law. The slope of this mixing length law appears as a simple linear function of a new pressure gradient parameter β', which, different from the usual β parameter, takes into account both the external and the friction velocities. This inner wake region shows a characteristic length scale that is different from the wall region length scale. This new length scale, which is of

inner type, together with previous results of the literature, emphasizes the role of the displacement thickness δ^* in adverse pressure gradient boundary layers.

To verify whether this new scaling is peculiar to the present flow or has more generality, the data from Ludwig and Tillman (see Ref. 3, pages 1100, 1101) were plotted in this representation. The mild adverse pressure gradient case was selected as a configuration comparable to the present one. The pressure gradient of this flow shows some similarity with the one in Fig. 5, but the Ludwig and Tillman experiment has no curvature effect. The results, which are not presented here, show that the proposed model fits fairly well with the data. The linear region appears again just above the log region and extends outward as the flow progresses downstream. The parameter D takes a constant value, which is fairly different from the present one (16.2 instead of 11.5). The coefficient χ also shows different behavior as it tends rapidly to a constant value of 2.5. This leads to the conclusion that these two coefficients are dependent on the flow under consideration and that more experiments should be analyzed to find their general behavior. Nevertheless, the results show again that the proposed scaling leads the velocity profiles to tend to universality as the flow progresses downstream. This behavior can be compared to jets and wakes where the self-similar region appears at some distance downstream of the origin of the considered flow.

To conclude, it appears that the external part of the wake on these velocity profiles does not follow usual wake laws. (Several attempts were made to fit them.) This region is interpreted here as a downstream persistence of the wake part of the incident flat plate BL that has been submitted to a strong favorable pressure gradient before the adverse pressure gradient region under study.

IV. Conclusions

An experiment has been devised to study the possibilities of flow control of a TBL submitted to an adverse pressure gradient. This situation is typical of the suction side of an airfoil (or a flap) at high angle of attack, and care was taken, by computing the shape of the model with a two-dimensional Navier–Stokes solver, to generate flow conditions representative of flight. The aim of the present paper was to present a detailed characterization of the basic flow before the actuation tests. For that purpose, wall pressure distribution and velocity profiles at five different stations were measured. The pressure distribution obtained appears to mimic precisely the one expected from the preliminary computations performed at Dassault Aviation. As happens on the suction side of an airfoil, in the diverging part, the flow is submitted to both an adverse pressure gradient and curvature. Although the model shows a straight diverging part of significant extent, the BL under study is far from the equilibrium conditions as defined in detail by Townsend.[9] This is clearly indicated by the evolution along the flow of the integral parameters of the BL. In fact, the present BL can be considered to be submitted to a mild adverse pressure gradient because at the end on the bump the shape factor H_{12} has a value of 1.7, which is not too near the separation value ($H_{12} \sim 2$). As compared for example to studies by Dengel and Fernholtz,[14] who were looking at phenomena around the separation region, the present experiment is more concerned with what happens at the early stage of the separation process, when the BL starts to encounter the adverse pressure gradient, far upstream of the separation point.

When the mean velocity and turbulence intensity (not shown here) profiles measured at five stations by single hot-wire anemometry are examined, it appears that an instability develops very early after the change of sign of the pressure gradient in the near-wall region. This instability is clearly detectable on the turbulence intensity profiles by a second peak, which develops just above the near-wall peak and rapidly overwhelms it. On the mean velocity profiles, the main consequence is a linear inner wake region, which develops above the log layer. A comparison with various proposals from the literature[14,20,21] shows that this region does not scale following previous proposals and, in particular, does not scale with external variables. The analysis does show that the friction velocity u_τ is still a relevant velocity scale in that region, whereas ν/u_τ, which is the usual length scale in the near-wall region, has to be replaced by $l \approx \delta^*(u_\tau/U_e)$ to obtain a universal representation of the linear part of the mean velocity profile. A far as turbulence modeling is concerned, as observed by most previous authors, a universal logarithmic region, witness of a linear variation of the mixing length, is observed at all stations. The size of this log region decreases along the flow. Just above the log region, in the linear part of the profile, a half-power mixing length law has been put in evidence, which allows the evolution of the velocity profiles to be predicted fairly well. It was also put to evidence that, at the first two stations, where the BL is still quite thin and energetic, the velocity profiles are influenced by the convex wall curvature. This is not true at the last station where the wall is concave, but the BL is much thicker and already strongly influenced by the adverse pressure gradient. To check the universality of the new scaling and mixing length proposed, they were applied to the reference experiment of Ludwig and Tillman.[2] The mild pressure gradient case was selected as comparable to the present experiment. The results show that the model fits quite well with these reference data in the inner wake region, but with different values of coefficients. As far as scaling is concerned, the two experiments show a tendency toward universality as the flow progresses downstream. This should be confirmed by a more extensive study of results available in the literature.

Acknowledgments

We are thankful to J. C. Courty and J. J. Valet from Dassault Aviation for providing the results of the Navier–Stokes computation. The research reported here was undertaken as part of the AEROMEMS project (an investigation of the viability of microelectromechanical systems technology for boundary-layer control on aircraft), which is a collaboration between British Aerospace, Dassault Aviation, Centre National de la Recherche Scientifique of Lille and Besançon, and the Universities of Athens, Berlin, Lausanne, Madrid, Manchester, and Tel Aviv. The project is managed by British Aerospace and partially funded by the EC under the IMT initiative (Project BRPR CT97-0573).

References

[1]Gad-El-Hak, M., "Introduction to Flow Control," *Flow Control-Fundamental and Practices*, edited by M. Gad-El-Hak, A. Pollard, and J.-P. Bonnet, Springer-Verlag, Berlin, 1998, pp. 1–107.

[2]Ludwig, H., and Tillman, W., "Investigations of the Wall Shearing Stress in Turbulent Boundary Layers," National Advisory Committee Aeronautics Washington, TM 1285, 1950.

[3]Coles, D. E., and Hirt, E. A. (eds.), *Proceedings of the AFOSR–IFP–Stanford Conference on Computation of Turbulent Boundary Layers*, Vol. 2, 1968, pp. 1100, 1101.

[4]Spalart, P. R., and Watmuff, J. H., "Experimental and Numerical Study of a Turbulent Boundary Layer with Pressure Gradients," *Journal of Fluid Mechanics*, Vol. 249, 1993, pp. 337–371.

[5]So, R. M. C., and Mellor, G. L., "Experiment on Turbulent Boundary Layer on Concave Wall," *Aeronautical Quarterly*, Vol. 26, 1975, pp. 25–40.

[6]Meroney, R. N., and Bradshaw, P., "Turbulent Boundary Layer Growth over a Longitudinally Curved Surface," *AIAA Journal*, Vol. 13, No. 11, 1975, pp. 1448–1453.

[7]Ramaprian, B. R., and Shivaprasad, B. G., "Mean Flow Measurements in Turbulent Boundary Layers Along Mildly Curved Surfaces," *AIAA Journal*, Vol. 15, No. 2, 1977, pp. 189–196.

[8]Coles, D. E., "The Law of the Wake in the Turbulent Boundary Layer," *Journal of Fluid Mechanics*, Vol. 1, 1956, pp. 191–226.

[9]Townsend, A. A., "Equilibrium Layers and Wall Turbulence," *Journal of Fluid Mechanics*, Vol. 12, 1961, pp. 97–120.

[10]Perry, A. E., Bell, J. B., and Joubert, P. N., "Velocity and Temperature Profiles in Adverse Pressure Gradient Turbulent Boundary Layers," *Journal of Fluid Mechanics*, Vol. 25, 1966, pp. 299–320.

[11]Perry, A. E., "Turbulent Boundary Layers in Decreasing Adverse Pressure Gradients," *Journal of Fluid Mechanics*, Vol. 26, 1966, pp. 481–506.

[12]Perry, A., and Shofield, W., "Mean Velocity and Shear Stress Distribution in Turbulent Boundary Layers," *Physics of Fluids*, Vol. 113, 1973, pp. 2068–2074.

[13]Samuel, A. E., and Joubert, P. N., "A Boundary Layer Developing in an Increasingly Adverse Pressure Gradient," *Journal of Fluid Mechanics*, Vol. 66, 1974, pp. 481–505.

[14]Dengel, P., and Fernholtz, H., "An Experimental Investigation of a Turbulent Boundary Layer in the Vicinity of Separation," *Journal of Fluid Mechanics*, Vol. 212, 1990, pp. 615–636.

[15]Skare, P. E., and Krogstad, P. A., "A Turbulent Boundary Layer near Separation," *Journal of Fluid Mechanics*, Vol. 272, 1994, pp. 319–348.

[16]Kasbarian, C., Lebigre, O., Mallet, M., Mantel, B., Ravachol, M., and Tintillier, M., "Development of a Finite Element Navier–Stokes Solver Using Unstructured Adapted Grids, Applications to Turbulent Flows," *Computational Fluid Dynamics'92*, edited by C. Hirsch, Vol. 1, 1992.

[17]Chalot, F., Mallet, M., and Ravachol, M., "A Comprehensive Finite Element Navier–Stokes Solver for Low and High-Speed Aircraft Design," AIAA Paper 94-0814, Jan. 1994.

[18]Trukenbrodt, E., "Ein Quadraturverfahren zur Berechnung der Laminaren und turbulenten Reibungsschicht bei Ebender und Rotationssymmetrischer Strömung," *Ingenieur Achiv*, Vol. 20, 1952, pp. 211–228.

[19]Schlichting, H., *Boundary Layer Theory*, 7th ed., McGraw–Hill, New York, 1979, p. 674.

[20]Cousteix, J., *Turbulence et Couche Limite*, Editions Cepadues, Toulouse, France, 1989.

[21]Durbin, P. A., and Belcher, S. E., "Scaling of Adverse Pressure Gradient Turbulent Boundary Layers," *Journal of Fluid Mechanics*, Vol. 238, 1992, pp. 699–722.

R. M. C. So
Associate Editor